11-2011

Estimation of velocity uncertainties from GPS time series: Examples from the Analysis of the South African TrigNet Network

Matthias Hackl
Ludwig-Maximilians-Universität

Rocco Malservisi
University of South Florida, rocco@usf.edu

Urs Hugentobler
Technische Universität München

Richard Wonnacott
National Geo-Spatial Inormation, Cape Town, South Africa

Estimation of velocity uncertainties from GPS time series: Examples from the analysis of the South African TrigNet network

M. Hackl,[1] R. Malservisi,[1,2] U. Hugentobler,[3] and R. Wonnacott[4]

Received 5 December 2010; revised 17 August 2011; accepted 18 August 2011; published 10 November 2011.

[1] We present a method to derive velocity uncertainties from GPS position time series that are affected by time-correlated noise. This method is based on the Allan variance, which is widely used in the estimation of oscillator stability and requires neither spectral analysis nor maximum likelihood estimation (MLE). The Allan variance of the rate (AVR) is calculated in the time domain and hence is not too sensitive to gaps in the time series. We derived analytical expressions of the AVR for different kinds of noises like power law noise, white noise, flicker noise, and random walk and found an expression for the variance produced by an annual signal. These functional relations form the basis of error models that have to be fitted to the AVR in order to estimate the velocity uncertainty. Finally, we applied the method to the South Africa GPS network TrigNet. Most time series show noise characteristics that can be modeled by a power law noise plus an annual signal. The method is computationally very cheap, and the results are in good agreement with the ones obtained by methods based on MLE.

Citation: Hackl, M., R. Malservisi, U. Hugentobler, and R. Wonnacott (2011), Estimation of velocity uncertainties from GPS time series: Examples from the analysis of the South African TrigNet network, *J. Geophys. Res.*, *116*, B11404, doi:10.1029/2010JB008142.

1. Introduction

[2] Satellite-based geodetic techniques provide an outstanding tool to measure crustal motions and deformations. Geodetically derived velocities of surface points provide necessary constraints to study tectonic plate motion, strain localization of active geological features, and to estimate rheological properties of the crust and the underlying asthenosphere [e.g., *Dixon*, 1991]. In general, geodetic velocities and their uncertainties are indirectly derived through repeated position measurements of given points.

[3] The measured relative position $x(t)$ of the point is the result of antenna motion and noise $\varepsilon(t)$. Any contribution to the measured antenna position is either modeled or considered to be noise. In geodynamics and tectonics the constant long-term (interseismic) rate is usually of major interest. Unfortunately, a constant long-term signal is not the only contribution to the antenna motion. Sudden (e.g., offset due to antenna changes or coseismic displacement), periodic (e.g., annual or semiannual seasonal deformations), or transient (e.g., postseismic deformation) signals are typically present in position time series. Some of the deviations from the long-term linear motion due to these contributions can be modeled and subtracted in order to improve the measured velocity of the observed point [*Segall*, 2010]. Still, the "corrected" time series remain affected by multiple sources of noise that cannot be completely removed from the signal (e.g., atmospheric delays, clock instability, monument motion, orbit error, etc.).

[4] *Johnson and Agnew* [1995], *Zhang et al.* [1997], *Mao et al.* [1999], and *Williams et al.* [2004] showed that GPS velocity uncertainties are underestimated by factors from 2 to 11 if only white noise (not time correlated noise) is considered. This suggests that time-correlated noise has to be taken into account in the calculation of velocity uncertainties.

[5] *Mao et al.* [1999] presented an error model that includes colored (time correlated) noise. Their empirical formula is based on spectral analysis and maximum likelihood estimation (MLE) of 23 globally distributed GPS stations with three years of data and takes into account flicker noise and random walk.

[6] *Williams* [2003a] also presented an empirical method to derive velocity uncertainties, followed by the presentation of CATS, a software package for the analysis of time series [*Williams*, 2008]. CATS can be used to perform a thorough time series analysis based on MLE for a variety of error models. A full analysis of the colored noise included in the time series through MLE is computationally expensive (depending on the error model up to $\mathcal{O}(n^3)$, for a time series of length n). *Bos et al.* [2008] presented an MLE approach that reduced the number of computations significantly ($\mathcal{O}(n^2)$

[1]Department of Earth and Environmental Sciences, Ludwig-Maximilians-Universität, Munich, Germany.
[2]Department of Geology, University of South Florida, Tampa, Florida, USA.
[3]Institute for Astronomical and Physical Geodesy, Technische Universität München, Munich, Germany.
[4]Chief Directorate: National Geo-spatial Information, Cape Town, South Africa.

0148-0227/11/2010JB008142

for a power law plus white noise error model), if there are no gaps in the time series. However, many published GPS velocity uncertainties are still computed assuming pure white noise or scaling the white noise by some empirical value derived from the repeatability of the time series [e.g., *Dixon et al.*, 2000]. Only in a few cases is time-correlated noise included, in general through the use of some empirical formula that does not require a full analysis of the time series [e.g., *Mao et al.*, 1999]. Still these methods can lead to both large overestimation and underestimation of the correct velocity uncertainty.

[7] There has been some debate on the choice of the error model and whether a random walk signal, mainly due to monument motion, is present in geodetic data or not. Continuous strainmeter and tiltmeter measurements at the Ida and Cecil Green Piñon Flat Observatory show a power law process close to random walk [*Wyatt*, 1982, 1989]. This is in agreement with geodimeter and trilateration measurements [*Langbein et al.*, 1987; *Langbein and Johnson*, 1997]. However, the analyses of *Zhang et al.* [1997] and *Mao et al.* [1999] suggest that flicker noise is the prevalent signal in GPS time series and random walk plays a secondary role. A comprehensive analysis of Southern California and South Nevada GPS sites by *Langbein* [2004, 2008] using MLE reveals that the time series are characterized by either flicker noise, random walk, general power law noise, or a combination of them and only in a few cases are these noises more complex including band-pass-filtered noise, first-order Gauss-Markov processes, or broadband seasonal noise. Recent studies by *Hill et al.* [2009] and *King and Williams* [2009] on short baselines, however, suggest that monument stability is not a dominant error source. *Santamaría-Gómez et al.* [2011] favor an error model consisting of white noise plus a power law noise, which is close to flicker noise for many sites. This is also in agreement with *Hill et al.* [2009] and *King and Williams* [2009].

[8] However, it is very difficult to distinguish between time-correlated noise and velocity variations from transient phenomena (like post seismic deformation). For example *Hackl et al.* [2009] showed that the long-term interseismic velocity field in Southern California (active plate boundary) can be affected by seismic cycle effects, which could explain a trend toward higher time correlation nearby active tectonic features.

[9] Here we present a method to estimate GPS velocity uncertainties. In contrast to the different scaling methods, our method accounts for site characteristics but does not require spectral analysis nor MLE. It is based on the Allan Variance, an analysis often used as a measurement of frequency stability in clocks and oscillators [*Allan*, 1966; *Barnes*, 1966; *Rutman*, 1978] and it is applied to the slope of the time series. As the calculation is done in the time domain, the method is not too sensitive to gaps in the data and it is computationally cheap. The method provides the variance of the rate as a function of the considered time span (up to ~1/4 of the total time series length) without any assumption of the noise characteristics. The method is an extension of the one suggested by *Caporali* [2003] to estimate the stability of time series as a function of time. It is tested with synthetic time series and finally applied to the South Africa GPS network TrigNet, a network almost not affected by tectonic deformation.

2. Time-Correlated Variance

[10] Like many geophysical phenomena, noise in GPS position time series can be described as a power law process [*Mandelbrot*, 1983; *Agnew*, 1992]. This one-dimensional stochastic process $\varepsilon(t)$ is characterized by a power spectrum of the form

$$P_x(f) = P_0 \left(\frac{f}{f_0}\right)^{\nu}, \tag{1}$$

where f is the temporal frequency, P_0 and f_0 are normalizing constants, and ν is the spectral index [*Mandelbrot and Van Ness*, 1968]. White noise corresponds to $\nu = 0$, flicker noise to $\nu = -1$, random walk to $\nu = -2$. There are many ways to deal with time-correlated noise mostly based on spectral analyses [e.g., *Lomb*, 1976; *Scargle*, 1982] or on MLE [e.g., *Williams*, 2008; *Bos et al.*, 2008]. Another way to deal with time-correlated noise was developed to calculate clock uncertainties and is called Allan variance or two-sample variance [*Allan*, 1966; *Barnes*, 1966; *Rutman*, 1978]. It is defined as one half of the average of the squared differences between consecutive readings of the observable sampled over a certain interval τ:

$$\sigma^2(\tau) = \frac{1}{2(n-1)} \sum_i (m_{i+1}(\tau) - m_i(\tau))^2 \tag{2}$$

where τ is the bin length, n the number of bins, and $m_i(\tau)$ the mean of the observable in the ith bin.

[11] The variance computed in this way is a function of the distribution being measured and the sample period. For stationary processes ($\nu > -1$) this variance is identical to the classical variance and thus it can be identified with the variance of the observable [*Allan*, 1966]. In the case of nonstationary processes the Allan variance for a certain bin length is independent of the time series length and the sampling frequency. Thus, the Allan variance is convergent in contrast to the classical variance. Although the meaning of a variance is questionable in the case of nonstationary processes the Allan variance still provides insights into the noise characteristics in those cases [*Allan*, 1987].

[12] The Allan variance has already been applied to geodetic time series to study uncertainties associated with site positions [*Le Bail*, 2004]. Here, the Allan variance has been modified in the sense that the mean of each bin is replaced by its slope. To avoid confusion we will call the variance computed in this way Allan Variance of the Rate (AVR). In simple terms, the time series is divided into n bins of equal length τ. Then the slope of the time series is calculated for every bin by linear regression. The AVR corresponding to a given τ is then defined as one half of the variance of the differences of the slopes of two consecutive bins. Figure 1 shows a synthetic time series and the corresponding AVR that is displayed in a log-log plot as a function of the bin length τ. The statistical significance of the AVR depends on the number of bin pairs used in the computation. In tests

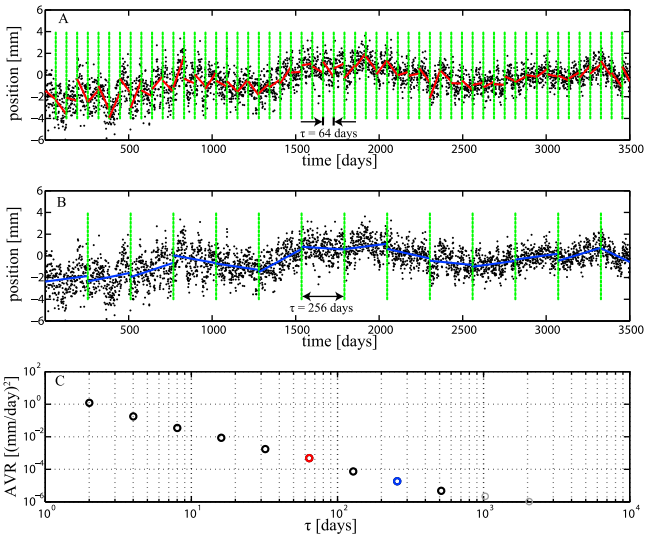

Figure 1. (a and b) Synthetic time series and (c) corresponding Allan variance of the rate (AVR). The time series is divided in n bins of length τ, and the slope of each bin is calculated by linear regression (red and blue lines in Figures 1a and 1b). The AVR is calculated using equation (2). The red circle at τ = 64 days corresponds to the bins shown in Figure 1a, and the blue circle at τ = 256 days corresponds to the bins shown in Figure 1b. The light grey circles in the AVR are based on less than four bin pairs; hence they are statistically poorly constrained and should not be included in the fit of an error model.

with synthetic time series reasonable results were obtained down to four bin pairs. The necessity of at least four bins to compute a statistical significant variance limits the maximum time span for which the variance can be directly computed to ~1/4 of the total length of the time series. The statistics of the AVR can be significantly improved at the expense of computational time for computing the AVR for overlapping bins [e.g., *Howe et al.*, 1981]. This requires more calculation steps, but provides better results in terms of statistical significance. The variance associated to the full series needs to be extrapolated assuming an error model. Still the AVR provides a visual representation of the improvement of the velocity uncertainty with increasing time length independently from the selected error model.

[13] Gaps in the time series do not dramatically affect the calculation of the AVR. We tested the method with synthetic time series where gaps were created removing up to 50% of the points and obtained very similar results compared to the corresponding time series without gaps. As an empirical rule derived by tests with synthetic time series we found that if a bin contains at least 30% of the data points and the time span covered in the bin is at least 50% of τ it can be included in the calculation. It is worthy to mention that it does not make a difference whether the time series is detrended or not since only the difference of slopes of consecutive bins is used. While the upper limit of the length of τ is specified by the time series length, the lower limit is specified by the sampling rate and numerical stability. Testing with synthetic time series we found that starting from bin length τ larger than four times the sampling rate improves the numerical stability of the calculation drastically.

3. Error Model

[14] The method described in section 2 provides the velocity uncertainty for any interval length of the time series within the accessible range of τ limited by the necessity of multiple bins to get a statistically significant value of the variance and by the sampling period ($4t < \tau < L/4$, where t is the sampling period and L the length of the time series). In most cases we want to assess the velocity uncertainty corresponding to the full length of the time series. In order to do so an error model based on assumptions on the noise characteristics is required and a corresponding function has to be adjusted to the slope variance. Its extrapolation to the full length of the time series can then be interpreted as the variance of the velocity of the full time series. The extrapolation requires a function based on assumptions on the noise characteristics. Unless a complete analysis of all noise contributions in GPS time series is considered, the choice of the right error model will be subject to debate. Here, some of the most common error models were applied to the AVR of synthetic time series, in order to validate the presented method.

3.1. Power Law Noise

[15] *Agnew* [1992] analyzed the time domain behavior of Gaussian power law noise (equation (1)) and derived the relation

$$\sigma_x(T) \propto T^{\frac{-(\nu+1)}{2}} \tag{3}$$

for the standard deviation σ_x of the position for a given time series with a spectral index ν and length T. This implies that for $\nu \leq -1$ the position uncertainty does not decrease with increasing the length of the time series, the process is not stationary. It has been shown [*Allan*, 1966; *Bos et al.*, 2008] that the variance σ^2 of the linear velocity v is proportional to

$$\sigma_v^2(T) \propto T^{-(\nu+3)} \tag{4}$$

In the case of Gaussian distributed noise this expression implies the linear relationship

$$\mu = -(\nu + 3) \tag{5}$$

between the spectral index ν and the slope μ of the AVR in a log-log plot (see Table 1). This relationship between μ and ν is also in agreement with *Williams* [2003a]. Unlike the position, the velocity information still improves with observation length for $\nu > -3$.

[16] In the case of a power law noise the AVR of the velocity as a function of the length of the time series can be modeled by

$$\sigma_v^2(T) = a_{pl} T^{\mu} \tag{6}$$

In order to test the presented method, 21,000 time series with spectral indices $-2 \leq \nu \leq 0$ were created and analyzed. A subset of 1000 points were taken from time series of 10,000 points to avoid boundary effects. All time series were generated as a superposition of Ornstein-Uhlenbeck

Table 1. Spectral Index ν and the Power-Law Index of the AVR μ for the Most Frequently Mentioned Noises With Gaussian Distribution

	ν	μ
White noise	0	−3
Flicker noise	−1	−2
Random walk	−2	−1

processes [*Kasdin*, 1995; *Milotti*, 2006]. The time series were also analyzed using CATS, a *psd* spectral analysis Matlab routine [*Stoica and Moses*, 1997; *Welch*, 1967; *Oppenheim and Schafer*, 1989], and a method introduced by *Lomb* [1976] and *Scargle* [1982]. The Matlab routine is based on the periodogram, which is a widely used, simple, and fast algorithm, although it is known to be a biased estimate [e.g., *Stoica and Moses*, 1997] and is included only for completeness.

[17] The results are summarized in Figure 2, showing the average and the dispersion of the difference between the estimated spectral index for the different methods and the spectral index utilized to create the time series. The error bars denote the standard deviation of the estimates. Although CATS is clearly the best performing method, it is evident that all the different methods are able to estimate the correct spectral index within the corresponding dispersion and with a relative accuracy smaller than 0.1. A bias in the psd method is clearly visible for low spectral indexes. We also note that the AVR tends to produce a slightly higher power spectrum at high spectral indices probably due to the numerical stability choice of starting the integration from $\tau > 4t$ (thus partially decreasing the contribution of white noise). We also note an increase in the dispersion of the results at lower spectral indices that is probably due to the necessity to limit the interpolation to τ not longer than 1/4 of the length of the time series.

3.2. White Noise, Flicker Noise, and Random Walk

[18] Previous studies [e.g., *Zhang et al.*, 1997; *Mao et al.*, 1999] suggested that the noise in GPS time series consists of a combination of white noise, flicker noise, and random walk. One reason for the use of these three particular noise contributions was that the derivations of the corresponding covariance matrices existed only for these integer spectral indices. Although today it is possible to derive the covariance matrix for any power law noise by fractional differencing and integrating, the estimation of the spectral index along with the noise magnitudes is computationally expensive. Therefore, most GPS velocity uncertainties are still calculated assuming an error model consisting of the aforementioned noise types.

[19] The method presented here is also able to deal with error models consisting of a combination of white noise, flicker noise, and random walk by using the relationship between spectral index and power law behavior of the AVR (equation (5)). For this error model the variance of the rate can be written as

$$\sigma^2_{wn+fl+rw}(\tau) = a_{wn}\tau^{-3} + a_{fl}\tau^{-2} + a_{rw}\tau^{-1} \qquad (7)$$

where a_{wn}, a_{fl}, and a_{rw} are the coefficients for white noise, flicker noise, and random walk, respectively. Table 1 summarizes the different noise types, their spectral indices and the corresponding AVR exponents.

[20] In the case of a linear combination of different noise types it is interesting to look at the values τ_{co}, where the slope of the AVR changes (crossover bin length). For these bin lengths the contribution of the corresponding noise types have the same magnitude. The τ_{co} separate regimes where the specific noise contributions are dominant. Noise processes with lower spectral indices, for example random walk, are dominant at larger bin lengths, while noise with a higher spectral index such as white noise is dominant for shorter bin lengths. Therefore error sources with a correspondingly small ν ($\nu \to -\infty$) can never be ruled out for finite time series since low spectral index processes may become dominant for bin lengths exceeding the length of the time series.

[21] Similarly to what we did for testing the power law model, synthetic time series consisting either of one noise type or a combination of different noise types were created. Then the AVR was computed. Finally, we adjusted the parameters a_{wn}, a_{fl}, and a_{rw} in the error model function (equation (7)) to fit the AVR (see Figure 3 and Table 2). In general we were able to estimate the correct noise contributions in the accessible range of bin lengths (a region bounded below by four times the sampling frequency and above by 1/4 of the length of the time series).

[22] As an example we can look at the case of "white noise + random walk" (Figure 3). Equation (7) was adjusted to the variances looking for the values of a_{wn}, a_{fl}, and a_{rw} that represent the calculated variances best. We used those parameters to extrapolate function (7) to the full length of the time series (red lines in Figure 3). This value is the velocity variance of the given time series. As expected for this particular synthetic time series with only white noise

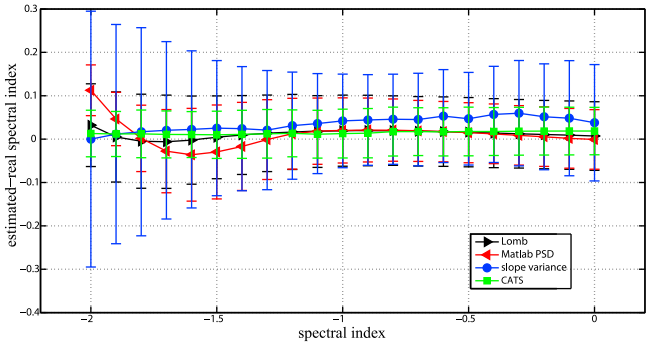

Figure 2. Estimated spectral indices with standard deviations from synthetic time series. The time series were created with a length of 10,000 days, but only 1000 were used in order to avoid boundary effects. The 1000 time series of each spectral index were created and analyzed by the AVR method introduced here. The spectral indices were estimated by a nonlinear fit weighting the data points by τ (blue). For comparison, 100 time series of each spectral index were analyzed by CATS (green), a Matlab-implemented function to calculate the power spectral density (red), and a method introduced by *Lomb* [1976] and *Scargle* [1982] (black). The latter two methods provide power spectra, and the spectral indices were calculated by linear regression of the log-log representation of the power spectra.

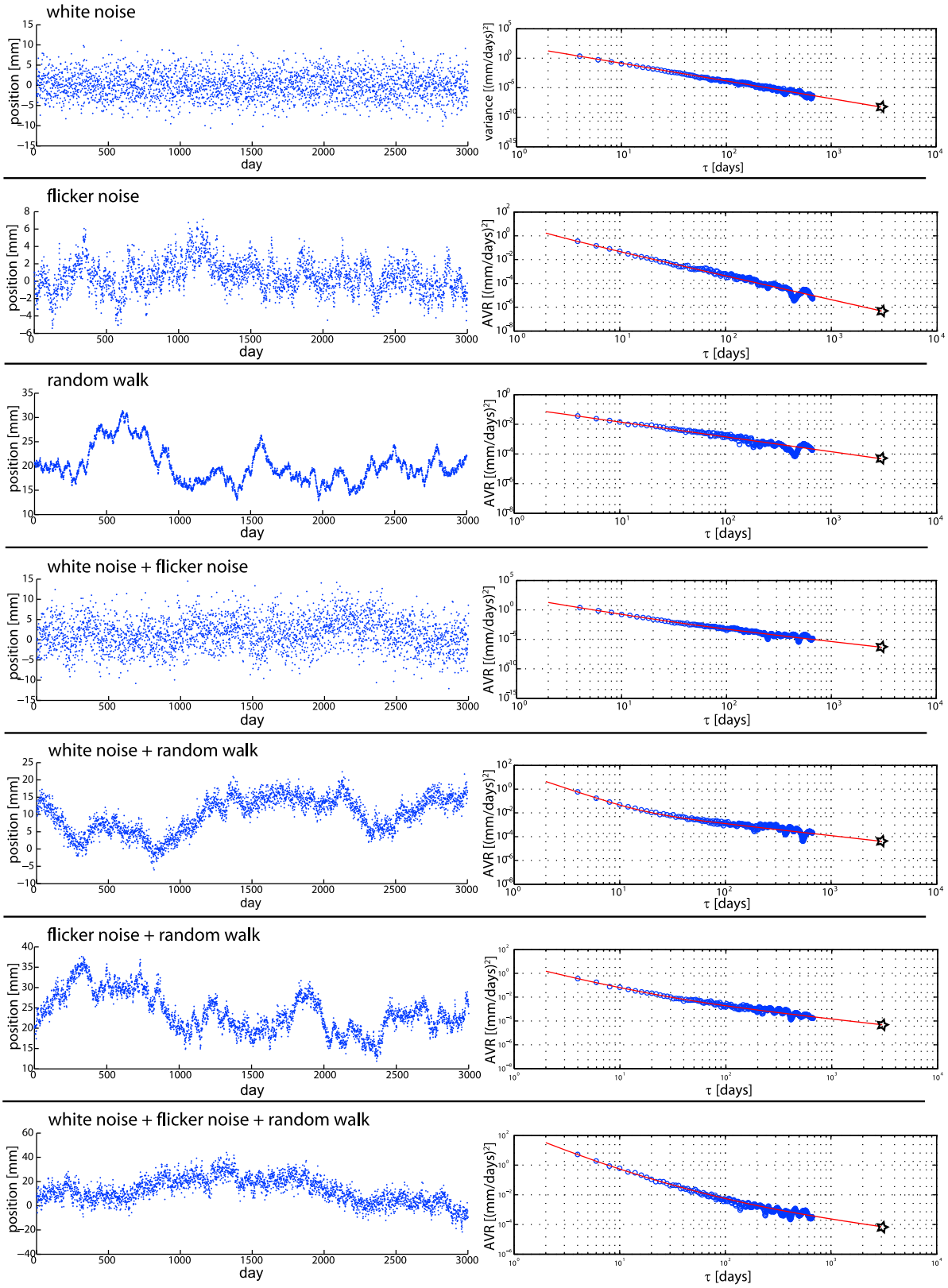

Figure 3. (left) Synthetic time series and (right) the corresponding AVRs. The time series consist of white noise, flicker noise, or random walk and any possible combination of these noise types. The coefficients in equation (7) (the error model; red lines, Figure 3 (right)) are estimated by least squares fitting to the variances based on more than four bin pairs (blue circles in variance plots) and are summarized in Table 2. The crossover periods τ_{co} (in days) confine intervals where the different noise contributions are dominant.

Table 2. Parameter Estimates of Example Time Series Shown in Figure 3

Noise	a_{wn} (mm^2/d)	a_{fl} (mm^2)	a_{rw} (mm^2/d)	τ_{co}(wn-fl) (days)	τ_{co}(fl-rw) (days)	τ_{co}(wn-rw) (days)	σ_v^2 (mm^2/yr^2)
White noise	142	2.22×10^{-14}	2.22×10^{-14}	6.38×10^{15}	1.00	7.99×10^{7}	0.026
Flicker noise	4.94	4.26	2.22×10^{-14}	1.16	1.92×10^{14}	1.49×10^{7}	0.25
Random walk	2.22×10^{-14}	2.22×10^{-14}	0.143	1.00	1.15×10^{-13}	3.34×10^{-7}	2.52
White noise plus flicker noise	136	4.17	2.22×10^{-14}	32.5	1.88×10^{14}	7.81×10^{7}	0.25
White noise plus random walk	34.7	2.22×10^{-14}	0.122	1.56×10^{15}	1.82×10^{-13}	169	2.33
Flicker noise plus random walk	2.21	4.67	0.143	0.473	32.8	4.01	2.53
White noise plus flicker noise plus random walk	191	33.6	0.204	5.69	165	30.6	3.09

and random walk the coefficient a_{fl} is negligible. For this particular time series, the crossover bin length of white noise and random walk $\tau_{co}(wn - rw)$ is 169 days. This means that for observations shorter than this time span white noise is the dominant noise contribution while for longer observations it is random walk. For flicker noise a virtually vanishing contribution is estimated and crossover bin lengths are thus meaningless.

3.3. Seasonal Effects

[23] Many GPS time series show annual signals mainly because of seasonal loading. In most cases the seasonal signals are just modeled by the first and the second harmonics of a sine function, where the fundamental period is one year. The signal is then subtracted from the time series. *Blewitt and Lavallée* [2002] showed that a seasonal signal still affects the velocity uncertainty and presented the following series to estimate the velocity uncertainty introduced by a seasonal signal:

$$\sigma^2_{annual}(\tau) = \frac{18T^2a_1^2}{\pi^2\tau^4}\sum_{k=1}^{\frac{T}{2\Delta t}}\frac{1}{k^3}\left(\cos\left(\frac{\pi k\tau}{T}\right) - \frac{T}{\pi k\tau}\sin\left(\frac{\pi k\tau}{T}\right)\right)^2 \quad (8)$$

where a_1 is the amplitude of the contribution at the fundamental period T, Δt is the sampling interval, and τ is the length of the time series. *Blewitt and Lavallée* [2002] indicated that the contributions with k = 1,2 (annual and semiannual) account for ~90% of the total variance. Equation (8) is limited to $\tau > T$, which makes it difficult to use it for fitting in the presence of noise since the adjustment should include the full range of τ. *Bos et al.* [2010] showed the importance of including the effect of colored noise when dealing with periodic signals.

[24] A periodic signal is not a stochastic process and as a consequence the AVR cannot directly be identified with the velocity variance. Here we discuss the effect of a periodic signal on the AVR and show how the method presented here can be used to estimate the amplitude at the fundamental period, which then can be used along with equation (8) to estimate correct velocity uncertainties. There are two advantages of doing so: (1) the amplitude is estimated along with other (colored) noise parameters and (2) the phase is not present in this formulation.

[25] The AVR for a pure sinusoidal signal of the form

$$x(t) = a\sin\left(\frac{2\pi}{T}t + \Phi\right) \quad (9)$$

where a is the amplitude of the signal, T its period, and Φ a phase can be calculated analytically with Maple (TM). The expression obtained is very complex and not suitable for fitting an error model, but it can be approximated by

$$\sigma^2_{annual}(\tau) = \frac{36T^2a^2}{\pi^2\tau^4}\sin^2\left(\frac{\pi\tau}{T}\right)\left(\frac{T}{\pi\tau}\sin\left(\frac{\pi\tau}{T}\right) - \cos\left(\frac{\pi\tau}{T}\right)\right)^2 \quad (10)$$

where a is the amplitude of the sinusoidal signal that can be solved for by fitting the data for a given period T (e.g., T = 365 days for an annual signal).

[26] Equation (10) is identical to the one derived by *Blewitt and Lavallée* [2002] for the velocity bias from a sinusoidal signal, apart from a phase not present on the AVR. The phase term is absent because the AVR is computed using the difference of consecutive bin pairs. At every phase of a harmonic signal the difference is zero at integer multiples of T independent from the phase. In this way, as long as we have enough bins, the phase bias to the AVR is averaged out.

[27] It is possible to apply the AVR and to fit an adequate model that accounts for the colored noise (like the ones described in 3.1 or 3.2) combined with the expression of the annual signal (equation (10)). By fitting the AVR to this model, a (that can be identified with a_1 in equation (8)) can be estimated along with the parameters describing the time-correlated noise (e.g., μ and a_{pl} in equation (6)). The values obtained by the fit can then be used in a linear combination of the selected noise model (e.g., equation (6)) and equation (8) to extrapolate the variance to the full length of the time series.

[28] As an example we created a synthetic time series consisting of flicker noise plus an annual signal of arbitrary phase. Figure 4 shows the time series (Figure 4, top) and the corresponding AVR (Figure 4, bottom). The red curve represents the adjusted model consisting of a linear combination of equations (6) and (10) corresponding to the parameters a_{pl}, μ, and a_1 that best reproduce the observed variance. The obtained parameter a_1 (corresponding to the amplitude of the sinusoidal signal) can now be used in the linear combination of equations (6) and (8) for extrapolation to the full length of the time series (black curve in Figure 4). The values of the black curve at the full time series length corresponds to the velocity variance when we take into account both colored noise and a periodic signal.

[29] Note, that for $\tau > T$ the variance introduced by an annual signal decreases with τ^{-4}, even faster than white noise.

3.4. Offsets and Velocity Changes

[30] Sometimes GPS time series are affected by offsets or changes in rates. Sources for offsets could include antenna changes or coseismic displacements. Velocity changes have

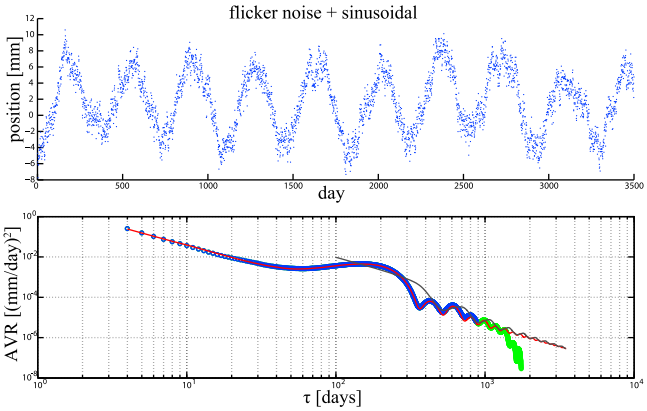

Figure 4. (top) Synthetic time series consisting of flicker noise plus a sinusoidal signal with period T = 365 days and amplitude a = 5 mm and (bottom) the corresponding AVR. Green circles are based on four or fewer independent bin pairs and thus are not included in the fitting. Blue circles are based on more than four bin pairs and were used to fit a linear combination of equations (6) and equation (10) (red line). The obtained values are a_{pl} = 3.9, μ = −2.0, and a_1 = 4.7, which compares well to the amplitude of the periodic signal. For extrapolation to the length of the time series the obtained parameters were set into a linear combination of equations (6) and (8) (black line). The calculated velocity uncertainty in this case is σ_v = 0.20 mm/yr.

been observed after large earthquakes but could also be related to other effects like monumentation or water pumping. These signals affect the AVR. Although no analytical expressions for these cases were derived, we want to point out some characteristics.

[31] An offset in the time series causes a change in trend of the AVR. In the case of "white noise + offset" the slope variance shows a similar behavior like a random walk process, which is in agreement with *Williams* [2003b]. If there is a change of rate in the time series, it is possible that the corresponding AVR of the rate shows a kink and increases with τ for a certain range of integration intervals.

[32] The above mentioned error models are not suitable for uncertainty estimation of time series affected by offsets or velocity changes since the models do not account for those effects. However, it is possible to identify corresponding patterns in the AVR and correct affected time series and/or apply different kinds of error models.

4. TrigNet

[33] TrigNet is a network of about 50 continuously operating GNSS base stations distributed throughout South Africa (see Figure 5). Data span up to nine years for most of the TrigNet sites and are freely available (http://www.trignet.co.za/). They were processed using the Bernese GPS Software, V5.0 [*Dach et al.*, 2007] using state of the art analysis strategies and standards. For consistency, orbit products from the CODE (Center for Orbit Determination in Europe) Analysis Center of the International GNSS Service (IGS) were used [*Dow et al.*, 2009]. Tracking data were analyzed in daily batches in ionosphere-free linear combination and phase ambiguities were resolved to integers. Two-hourly troposphere zenith delay and daily gradient parameters were estimated for each station. Station velocities were retrieved by combining daily solutions at the normal equation level. Some 30 IGS stations were included into the network to realize the geodetic datum.

[34] The obtained velocities were rotated into a South Africa fixed reference frame by an Euler rotation minimizing the velocity residuals [*Malservisi et al.*, 2008]. Most residual velocities are <1 mm/yr (Table 3), as expected for an Archean cratonic region not affected by tectonic deformation. In order to solve for any internal deformation the velocity uncertainty is crucial. In theory, the residuals with respect to the stable region like South Africa should be of the same order of magnitude as the error. The formal error is about 0.01–0.02 mm/yr for the horizontal components of most sites, a magnitude smaller than the observed residuals, suggesting a clear signal in the observed velocity field. Given the almost random distribution of the azimuth of the residuals we expect that for the majority of the sites this is not the case and that the error is largely underestimated because the formal error neglects time-correlated noise.

[35] On the other hand, the application of the method introduced by [*Mao et al.*, 1999] produced errors significantly larger (almost 1 order of magnitude) than the residuals indicating that the uncertainties of the velocity field are overestimated. Given the importance of the associated error in the interpretation of such small residuals, it is clearly important to make a more complete analysis of the uncertainty associated with the studied velocity field. The AVR provides a quick method to improve the error estimation. Given the availability of specific algorithms to compute time-correlated uncertainties for GPS velocities like CATS, the algorithm presented by *Bos et al.* [2008], or the one presented here we strongly suggest that neither pure white noise models nor empirical methods [e.g., *Mao et al.*, 1999] should be used for the estimation of velocity uncertainties

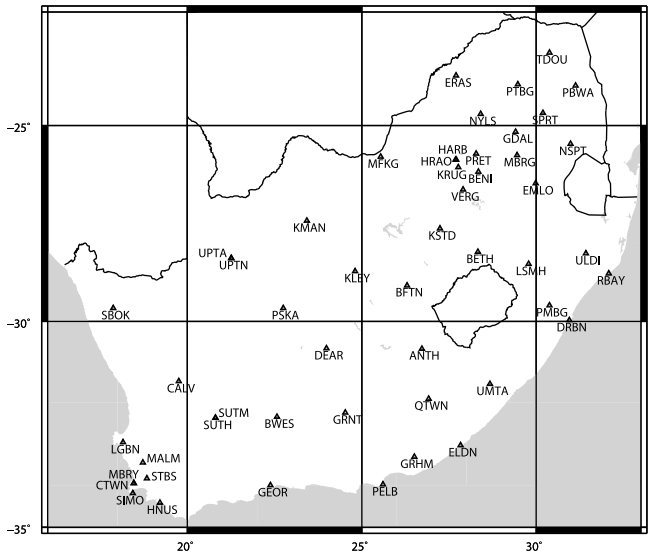

Figure 5. Spatial distribution of the South African GPS network TrigNet.

Table 3. TrigNet Residual Velocities, Their Uncertainties, and the Corresponding Spectral Indices[a]

Site	Longitude (deg)	Latitude (deg)	Length (days)	Completeness	v_{east} (mm/yr)	v_{north} (mm/yr)	σ_{east}^{CATS} (mm/yr)	σ_{north}^{CATS} (mm/yr)	σ_{east}^{AVR} (mm/yr)	σ_{north}^{AVR} (mm/yr)	ν_{CATS} East	ν_{CATS} North	ν_{AVR} East	ν_{AVR} North
HRAO	27.69	−25.89	3374	0.89	−0.51	−0.20	0.09	0.06	0.05	0.05	−0.59	−0.59	−0.31	−0.45
SUTH	20.81	−32.38	3372	0.90	0.18	0.11	0.10	0.05	0.46	0.06	−0.78	−0.60	−1.31	−0.60
HNUS	19.22	−34.42	3320	0.67	−0.08	−0.06	0.04	0.05	0.05	0.06	−0.40	−0.47	−0.43	−0.47
GEOR	22.38	−34.00	3274	0.52	−0.77	−0.27	0.05	0.04	0.05	0.07	−0.65	−0.59	−0.58	−0.64
PELB	25.61	−33.98	3267	0.51	0.02	−0.03	0.07	0.18	0.15	0.32	−0.75	−1.00	−0.90	−1.06
ELDN	27.83	−33.04	3266	0.70	−0.20	−0.05	0.04	0.04	0.03	0.05	−0.57	−0.55	−0.42	−0.55
BFTN	26.30	−29.10	3185	0.61	2.59	−1.18	0.29	0.09	1.83	0.47	−1.17	−0.85	−1.80	−1.34
UMTA	28.67	−31.55	3164	0.71	0.49	−0.24	0.03	0.05	0.02	0.04	−0.48	−0.65	−0.27	−0.39
BETH	28.33	−28.25	3164	0.78	−0.13	−0.04	0.03	0.03	0.03	0.05	−0.48	−0.52	−0.33	−0.57
PMBG	30.38	−29.60	3159	0.44	0.20	−0.12	0.05	0.04	0.05	0.04	−0.60	−0.55	−0.51	−0.36
LSMH	29.78	−28.56	3159	0.62	0.15	0.13	0.03	0.04	0.02	0.03	−0.45	−0.54	−0.23	−0.39
KLEY	24.81	−28.74	3159	0.60	0.27	−0.03	0.11	0.04	0.11	0.10	−0.80	−0.55	−0.70	−0.78
DRBN	30.95	−29.97	3155	0.57	0.27	−0.12	0.05	0.05	0.03	0.08	−0.60	−0.65	−0.35	−0.64
HARB	27.71	−25.89	3150	0.88	−0.07	0.07	0.05	0.06	0.03	0.07	−0.62	−0.63	−0.30	−0.61
SBOK	17.88	−29.67	3134	0.79	−0.02	−0.31	0.06	0.06	0.05	0.08	−0.63	−0.68	−0.53	−0.64
DEAR	23.99	−30.67	3125	0.67	−0.10	−0.20	0.03	0.04	0.02	0.08	−0.55	−0.64	−0.28	−0.72
CALV	19.76	−31.48	3125	0.77	−0.27	−0.11	0.09	0.07	0.16	0.12	−0.76	−0.65	−0.89	−0.75
ULDI	31.42	−28.29	3108	0.66	0.24	0.00	0.04	0.06	0.03	0.11	−0.49	−0.64	−0.28	−0.76
RBAY	32.08	−28.80	3098	0.50	0.27	−0.30	0.06	0.05	0.11	0.03	−0.57	−0.54	−0.78	−0.21
LGBN	18.16	−32.97	3003	0.71	0.18	0.02	0.05	0.06	0.06	0.11	−0.64	−0.69	−0.59	−0.80
ERAS	27.70	−23.69	2949	0.64	−0.06	−0.23	0.05	0.05	0.03	0.05	−0.55	−0.55	−0.23	−0.42
MBRG	29.45	−25.77	2927	0.71	0.14	0.72	0.09	0.09	0.10	0.17	−0.76	−0.75	−0.74	−0.94
PTBG	29.47	−23.92	2924	0.62	−0.26	0.23	0.06	0.04	0.12	0.06	−0.62	−0.52	−0.78	−0.54
NSPT	30.98	−25.48	2879	0.72	−0.04	0.05	0.06	0.11	0.06	0.25	−0.63	−0.81	−0.54	−1.00
PBWA	31.13	−23.95	2843	0.71	0.32	0.00	0.07	0.06	0.07	0.04	−0.67	−0.63	−0.56	−0.45
SIMO	18.44	−34.19	2703	0.51	−0.58	0.10	0.04	0.09	0.06	0.10	−0.34	−0.60	−0.41	−0.50
SUTM	20.81	−32.38	2578	0.92	−0.21	0.20	0.04	0.05	0.03	0.07	−0.45	−0.61	−0.26	−0.60
EMLO	29.98	−26.50	2561	0.78	−0.03	0.01	0.04	0.09	0.06	0.11	−0.54	−0.77	−0.57	−0.78
KMAN	23.43	−27.46	2531	0.79	0.20	−0.12	0.05	0.07	0.06	0.10	−0.59	−0.67	−0.51	−0.70
KSTD	27.24	−27.66	2529	0.61	−0.18	−0.42	0.06	0.05	0.11	0.06	−0.64	−0.58	−0.72	−0.53
MFKG	25.54	−25.81	2456	0.56	0.19	1.49	0.06	0.12	0.11	0.17	−0.60	−0.86	−0.79	−0.93
ANTH	26.72	−30.68	2260	0.77	0.02	0.20	0.05	0.06	0.07	0.08	−0.53	−0.59	−0.57	−0.61
TDOU	30.38	−23.08	2106	0.71	0.26	−1.89	0.12	0.15	0.29	0.39	−0.77	−0.85	−0.99	−1.11
GRNT	24.53	−32.25	2092	0.59	0.61	−0.05	0.09	0.07	0.03	0.04	−0.61	−0.46	−0.02	−0.12
BWES	22.57	−32.35	1987	0.56	0.34	0.20	0.17	0.08	0.06	0.08	−0.65	−0.54	−0.14	−0.46
PRET	28.28	−25.73	1901	0.83	0.16	−1.62	0.07	0.12	0.06	0.65	−0.59	−0.79	−0.45	−1.43
PSKA	22.75	−29.67	1694	0.85	0.14	−0.03	0.11	0.08	0.06	0.10	−0.66	−0.60	−0.18	−0.58
QTWN	26.92	−31.91	1679	0.78	0.74	1.15	0.16	0.15	0.54	0.31	−0.77	−0.75	−1.18	−0.90
NYLS	28.41	−24.70	1307	0.73	0.04	−0.17	0.09	0.08	0.14	0.11	−0.49	−0.43	−0.57	−0.46
GDAL	29.41	−25.16	1307	0.47	−0.10	0.57	0.11	0.08	0.12	0.09	−0.54	−0.47	−0.26	−0.35
MBRY	18.47	−33.95	1266	0.48	−0.07	0.23	0.17	0.33	0.08	0.11	−0.34	−0.52	0.11	0.15
GRHM	26.51	−33.32	1177	0.79	−0.07	0.23	0.07	0.27	0.11	0.39	−0.45	−0.81	−0.53	−0.85
UPTN	21.26	−28.41	1039	0.68	0.32	−0.68	0.14	0.17	0.12	0.12	−0.55	−0.64	−0.23	−0.27
SPRT	30.19	−24.67	969	0.89	2.04	−0.73	0.43	0.69	0.48	0.38	−0.84	−1.03	−0.78	−0.21
MALM	18.73	−33.46	850	0.85	0.18	0.06	0.16	0.15	0.20	0.19	−0.50	−0.48	−0.40	−0.42
STBS	18.84	−33.84	841	0.89	0.04	0.79	0.16	0.18	0.19	0.18	−0.50	−0.57	−0.40	−0.32
BENI	28.34	−26.20	794	0.87	6.66	2.71	0.51	0.22	0.67	0.30	−0.85	−0.59	−0.24	−0.38
KRUG	27.77	−26.08	791	0.86	0.03	−2.13	1.21	0.46	1.78	0.92	−1.21	−0.93	−1.19	−1.05
VERG	27.90	−26.66	788	0.91	−0.99	0.79	0.13	0.18	0.24	0.24	−0.43	−0.55	−0.52	−0.51
CTWN	18.47	−33.95	628	0.93	−0.07	0.23	0.37	1.25	0.54	1.12	−0.30	−0.69	−0.30	−0.30
UPTA	21.26	−28.41	508	0.87	0.18	−0.45	0.23	0.39	0.24	0.36	−0.41	−0.66	−0.19	−0.32

[a]Length indicates the time span covered by the time series. The uncertainties were calculated using CATS and the AVR method presented here. The formal error is on the order of 0.01–0.02 mm/yr in most cases.

from continuous GPS or semipermanent sites with sufficient amount of data.

5. CATS Versus AVR

[36] In order to estimate correct velocity uncertainties for the TrigNet time series CATS and the AVR method were applied. For both methods the same error model consisting of a power law noise plus an annual signal was used. The three components were treated independently in the calculation of the uncertainty, which is common practice. For the majority of the sites the spectral indices computed for the three components of the velocity are very similar, indicating that all the components are subject to the similar type of noise.

[37] In the case of the AVR an error model consisting of a linear combination of equations (6) and (10) was adjusted to the variances, solving for the parameters a_{pl}, μ, and a_1 by weighted nonlinear least squares. In order to improve the numerical stability of the least squares fit, only bins with lengths $\tau > 6$ days were included in the parameter estimation. To put more importance to the variances at greater τ and to stabilize the estimation of the parameters the computed variances were weighted by τ. In tests with synthetic

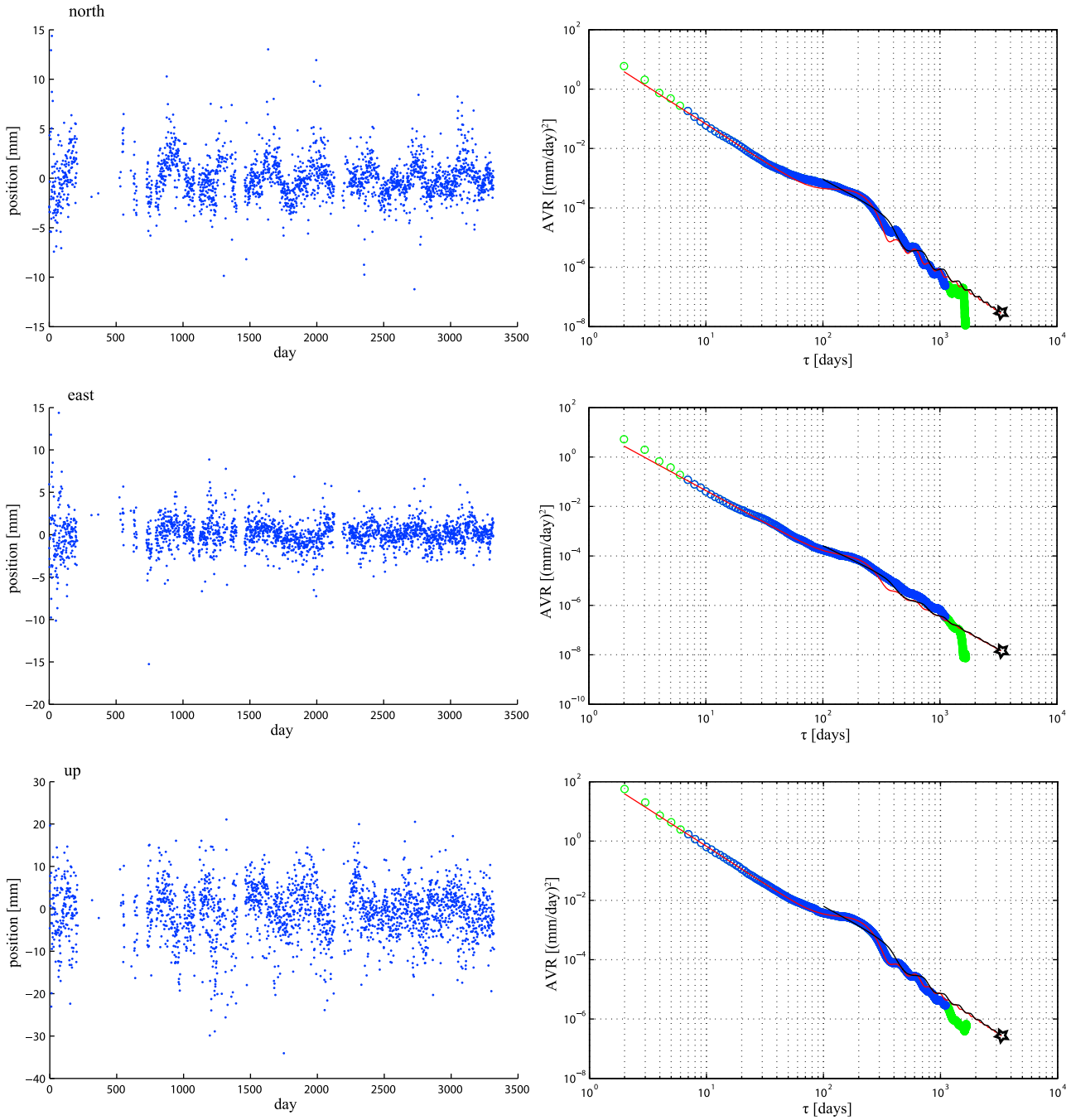

Figure 6. (left) Time series and (right) corresponding AVRs (green and blue circles) of the velocities for the three components of the GPS site at Hermanus (HNUS), South Africa. Variances that are based on more than six bin pairs (blue circles) were used to fit an error model (red line), which consists of a linear combination of power law noise (equation (6)) and an annual signal (equation (10)). The following parameters were obtained: a_{pl} (north) = 22.3, μ (north) = −2.53, a_1 (north) = 1.32, a_{pl} (east) = 16.3, μ (east) = −2.57, a_1 (east) = 0.58, a_{pl} (up) = 225, μ (up) = −2.53, and a_1 (up) = 3.26. The rate uncertainty is the result of the extrapolation of the black curve (see Figure 4). The stars in the variance plots denote the variances of the velocities; the corresponding standard deviations are σ (north) = 0.065 mm/yr, σ (east) = 0.045 mm/yr, and σ (up) = 0.053 mm/yr.

time series this weighting clearly improved the parameter estimation. This method is similar to the use of the logarithm of the data, a common practice in inversion methods when dealing with data with very different scales. Finally, the velocity uncertainties were estimated by extrapolating the linear combination of equations (6) and (8) to the full length of the time series. As an example, Figure 6 shows the time series and the corresponding slope variance at Hermanus (HNUS).

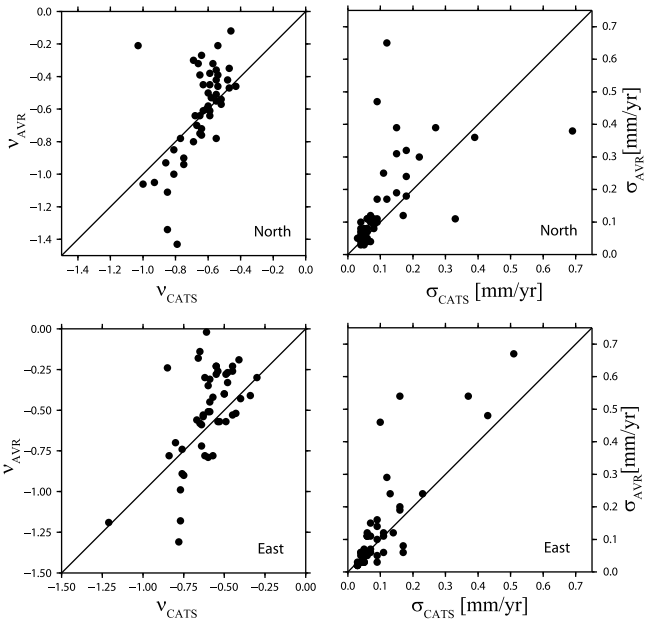

Figure 7. Scatterplots of (left) the spectral indices and (right) the calculated velocity uncertainties of (top) the north and (bottom) the east components of the TrigNet data set using CATS and AVR.

[38] In general, the calculations led to comparable results for both methods as summarized in Table 3 and Figure 7. Note, that the calculation times are significantly different, on a standard desktop PC (Dual Core 2.93 GHz, 4 GB RAM) the analysis of the network using CATS takes several days, while it takes only a few minutes (hours in the case of overlapping bins) to calculate the uncertainties using the AVR of the rate.

[39] The results calculated with the Allan variance tend to be slightly more conservative. A possible reason for this difference could be how white noise, that is likely to be present in the time series, is treated in the two methods.

[40] The shift toward higher uncertainties in our method becomes more apparent for sites with larger uncertainty σ, probably because these time series are in general shorter thus more influenced by white noise. Another reason for discrepancies of the two methods could be non Gaussian noise. The estimation of the spectral index in our method is based on the assumption of Gaussian distributed noise and the result could deviate from the one obtained by a different method.

[41] In general, the results of the two methods are more similar in cases where the selected error model fits well the computed AVR (i.e., the red curve fits well the blue dots in the variance plots like in Figure 6). This behavior emphasizes the importance of the right choice of the error model

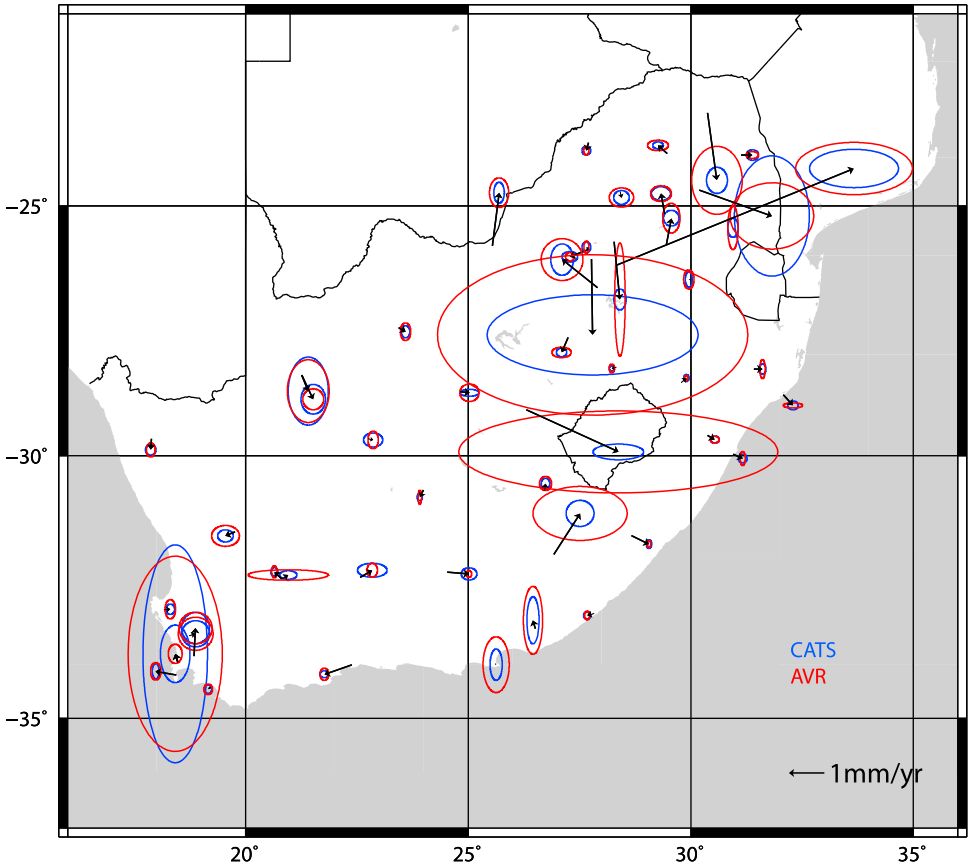

Figure 8. Horizontal residual velocity field of the South African GPS network TrigNet. The velocities are plotted with two error ellipses (95% confidence interval) corresponding to the different methods of uncertainty estimation (see Table 3). Blue ellipses correspond to the uncertainties calculated with CATS, and red ellipses correspond to the uncertainties calculated by the AVR method.

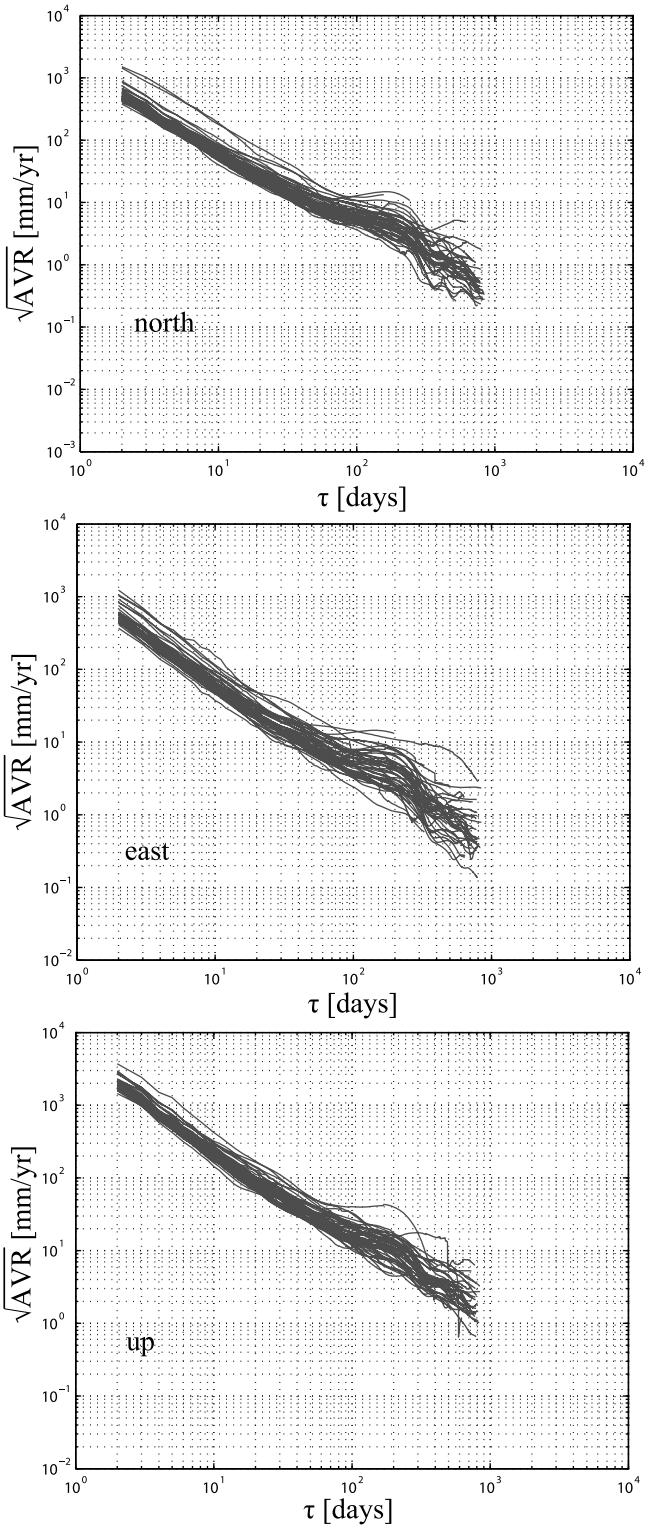

Figure 9. Standard deviations of the rates for three components of the TrigNet sites as a function of bin length. Most of the sites show an almost linear behavior in the log-log plot and a bump at $\tau \approx 183$ days. The shapes of most of the curves are similar, indicating similar sources of noise for the majority of the sites, which is also true for the different components.

and also shows the potential of the AVR to visually check whether an error model is suitable or not.

6. Conclusion

[42] Although CATS provides a broad set of different error models and a more robust estimation of the velocity uncertainty being based on MLE, the method presented here gets similar results and is faster for many choices of error models. The computation time is on the same order than for the algorithm presented by *Bos et al.* [2008] in the case of overlapping bins. The AVR has also the advantage to separate the estimation of the velocity uncertainty into two independent steps. First the variance is calculated as a function of varying bin length. In a second step an error model is used to compute the velocity uncertainty. This provides the possibility to choose an error model according to the computed variances and eventually the possibility to change the model in the case that the fit of the variance is not satisfactory without having to redo the full analysis. It is thus possible to dedicate more effort in the choice and the adjustment of the error model.

[43] Once the error is estimated correctly, the residual velocities for the TrigNet GPS network are of the same order than the estimated uncertainties for the majority of the sites in Figure 8, as expected for stable rigid plate setting. Some of the sites do still present significant residuals. In particular, some sites in the region around Johannesburg (e.g., HRAO) show a clear velocity signal that is likely caused by human induced deformation. Sites in the northeastern part of South Africa (e.g., PBWA or ULDI) have significant eastward residuals possibly associated with the deformation at the complex plate boundary between the Nubian and Somalian plates [*Stamps et al.*, 2008]. We also want to point out that some of the residuals can be associated with monumentation problems. In particular, PRET is installed on an unstable building, while QTWN and GEOR are combinations of multiple sites loosely connected by survey ties. BFTN and TDOU show high temporal correlations and relatively large errors, which could be related to local hydrological effects or monumentation problems. It is important to note that this interpretation of the velocity field as tectonic or nontectonic deformation is only possible after a correct estimation of the effects of time-correlated noise on the velocity uncertainties.

[44] Figure 9 shows the standard deviations of the velocities for the three components of the TrigNet sites. As expected for sites that are subject to similar noise the shapes of the curves are quite similar for the different sites, but also for the three components with the up component being shifted toward larger uncertainties. The bump at $\tau \approx 183$ days that is present in most of the curves results from the seasonal signal present in the time series. Apart from that the almost linear behavior in the log-log plot indicates that a power law assumption is reasonable, although a trend to convexity is present in some curves suggesting a piecewise power law behavior. The curves of a few sites differ significantly from the average shape and are very likely subject to additional processes. They possibly require additional processing and modeling and the velocities obtained should be handled with special care. Note, that the method presented here provides this kind of analysis independently of assumptions on the error model.

[45] **Acknowledgments.** We used data provided by the National Geo-spatial Information, Mowbray, South Africa, and the International GNSS Service (IGS). GPS analyses were performed with the BERNESE GPS software. This research benefitted from the availability of IGS data products. Figures were created using Matlab and the GMT software [*Wessel and Smith*, 1991]. We appreciate the constructive comments of Shimon Wdowinski and three anonymous reviewers, which improved the manuscript significantly. This study was funded by DFG grants MA 4163/1-1 and MA 4163/1-2. M.H. is supported by the Elitenetzwerk Bayern and different research projects of Valerian Bachtadse.

References

Agnew, D. C. (1992), The time-domain behavior of power-law noises, *Geophys. Res. Lett.*, *19*(4), 333–336.

Allan, D. W. (1966), Statistics of atomic frequency standards, *Proc. IEEE*, *54*(2), 221–230.

Allan, D. W. (1987), Should the classical variance be used as a basic measure in standards metrology?, *IEEE Trans. Instrum. Meas.*, *36*, 646–654.

Barnes, J. A. (1966), Atomic timekeeping and the statistics of precision signal generators, *Proc. IEEE*, *54*(2), 207–220.

Blewitt, G., and D. Lavallée (2002), Effect of annual signals on geodetic velocity, *J. Geophys. Res.*, *107*(B7), 2145, doi:10.1029/2001JB000570.

Bos, M. S., R. M. S. Fernandes, S. D. P. Williams, and L. Bastos (2008), Fast error analysis of continuous GPS observations, *J. Geod.*, *82*(3), 157–166, doi:10.1007/s00190-007-0165-x.

Bos, M., L. Bastos, and R. Fernandes (2010), The influence of seasonal signals on the estimation of the tectonic motion in short continuous GPS time-series, *J. Geodyn.*, *49*, 205–209, doi:10.1016/j.jog.2009.10.005.

Caporali, A. (2003), Average strain rate in the Italian crust inferred from a permanent GPS network—I. Statistical analysis of the time-series of permanent GPS stations, *Geophys. J. Int.*, *155*(6), 241–253, doi:10.1046/j.1365-246X.2003.02034.x.

Dach, R., U. Hugentobler, P. Fridez, and M. Meindl (2007), Bernese GPS software, version 5.0, user manual, Astron. Inst., Univ. of Bern, Bern.

Dixon, T. H. (1991), An introduction to the Global Positioning System and some geological applications, *Rev. Geophys.*, *29*, 249–276, doi:10.1029/91RG00152.

Dixon, T. H., S. Robaudo, J. J. Lee, and M. C. Reheis (2000), Present-day motion of the Sierra Nevada block and some tectonic implications for the Basin and Range province, North American Cordillera, *Tectonics*, *14*(4), 755–772.

Dow, J. M., R. E. Neilan, and C. Rizos (2009), The International GNSS Service in a changing landscape of Global Navigation Satellite Systems, *J. Geod.*, *83*, 191–198, doi:10.1007/s00190-008-0300-3.

Hackl, M., R. Malservisi, and S. Wdowinski (2009), Strain patterns from dense GPS networks, *Nat. Hazards Earth Syst. Sci.*, *9*(4), 1177–1187.

Hill, E. M., J. L. Davis, P. Elósegui, B. P. Wernicke, E. Malikowski, and N. A. Niemi (2009), Characterization of site-specific GPS errors using a short-baseline network of braced monuments at Yucca Mountain, southern Nevada, *J. Geophys. Res.*, *114*, B11402, doi:10.1029/2008JB006027.

Howe, D. A., D. W. Allan, and J. A. Barnes (1981), Properties of signal sources and measurement methods, in *Proceedings of the 35th Annual Symposium on Frequency Control*, pp. 669–716, Electr. Ind. Assoc., Washington, D. C.

Johnson, H. O., and D. C. Agnew (1995), Monument motion and measurements of crustal velocities, *Geophys. Res. Lett.*, *22*(21), 2905–2908, doi:10.1029/95GL02661.

Kasdin, N. J. (1995), Discrete simulation of colored noise and stochastic processes and $1/f^{\alpha}$ power law noise generation, *Proc. IEEE*, *83*(5), 802–827, doi:10.1109/5.381848.

King, M. A., and S. D. P. Williams (2009), Apparent stability of GPS monumentation from short-baseline time series, *J. Geophys. Res.*, *114*, B10403, doi:10.1029/2009JB006319.

Langbein, J. (2004), Noise in two-color electronic distance meter measurements revisited, *J. Geophys. Res.*, *109*, B04406, doi:10.1029/2003JB002819.

Langbein, J. (2008), Noise in GPS displacement measurements from southern California and southern Nevada, *J. Geophys. Res.*, *113*, B05405, doi:10.1029/2007JB005247.

Langbein, J., and H. Johnson (1997), Correlated errors in geodetic time series: Implications for time-dependent deformation, *J. Geophys. Res.*, *102*(B1), 591–603.

Langbein, J. O., M. F. Linker, A. F. McGarr, and L. E. Slater (1987), Precision of two-color geodimeter measurements: Results from 15 months of observations, *J. Geophys. Res.*, *92*(B11), 11,644–11,656, doi:10.1029/JB092iB11p11644.

Le Bail, K. (2004), Etude statistique de la stabileté des stations de géodésie spatiale: Application à DORIS, Ph.D. thesis, Inst. Géogr. Natl., Saint-Mandé, France.

Lomb, N. R. (1976), Least-squares frequency analysis of unequally spaced data, *Astrophys. Space Sci.*, *39*, 447–462, doi:10.1007/BF00648343.

Malservisi, R., U. Hugentobler, R. Wonnacott, and R. Chacko (2008), How rigid is a rigid plate? Geodetic constraint from the Kalahari craton, South Africa, paper presented at General Assembly 2008, Eur. Geosci. Union, Vienna.

Mandelbrot, B. B. (1983), *The Fractal Geometry of Nature*, W. H. Freeman, San Francisco, Calif.

Mandelbrot, B. B., and J. W. Van Ness (1968), Fractional Brownian motions, fractional noises and applications, *SIAM Rev.*, *10*(4), 422–437.

Mao, A., C. G. A. Harrison, and T. H. Dixon (1999), Noise in GPS coordinate time series, *J. Geophys. Res.*, *104*(B2), 2797–2816.

Milotti, E. (2006), PLNoise: A package for exact numerical simulation of power-law noises, *Comput. Phys. Commun.*, *175*, 212–225.

Oppenheim, A. V., and R. W. Schafer (1989), *Discrete-Time Signal Processing*, Prentice Hall, Englewood Cliffs, N. J.

Rutman, J. (1978), Characterization of phase and frequency instabilities in precision frequency sources: Fifteen years of progress, *Proc. IEEE*, *66*(9), 1048–1075.

Santamaría-Gómez, A., M.-N. Bouin, X. Collilieux, and G. Wöppelmann (2011), Correlated errors in GPS position time series: Implications for velocity estimates, *J. Geophys. Res.*, *116*, B01405, doi:10.1029/2010JB007701.

Scargle, J. D. (1982), Studies in astronomical time series analysis. II—Statistical aspects of spectral analysis of unevenly spaced data, *Astrophys. J.*, *263*, 835–853, doi:10.1086/160554.

Segall, P. (2010), *Earthquake and Volcano Deformation*, Princeton Univ. Press, Princeton, N. J.

Stamps, D. S., E. Calais, E. Saria, C. Hartnady, J.-M. Nocquet, C. J. Ebinger, and R. M. Fernandez (2008), A kinematic model for the East African Rift, *Geophys. Res. Lett.*, *35*, L05304, doi:10.1029/2007GL032781.

Stoica, P., and R. L. Moses (1997), *Introduction to Spectral Analysis*, Prentice Hall, Upper Saddle River, N. J.

Welch, P. (1967), The use of fast Fourier transform for the estimation of power spectra: A method based on time averaging over short, modified periodograms, *IEEE Trans. Audio Electroacoust.*, *15*(2), 70–73, doi:10.1109/TAU.1967.1161901.

Wessel, P., and W. H. F. Smith (1991), Free software helps map and display data, *Eos Trans. AGU*, *72*, 441, doi:10.1029/90EO00319.

Williams, S. D. P. (2003a), The effect of coloured noise on the uncertainties of rates estimated from geodetic time series, *J. Geod.*, *76*(9–10), 483–494, doi:10.1007/s00190-002-0283-4.

Williams, S. D. P. (2003b), Offsets in Global Positioning System time series, *J. Geophys. Res.*, *108*(B6), 2310, doi:10.1029/2002JB002156.

Williams, S. D. P. (2008), CATS: GPS coordinate time series analysis software, *GPS Solutions*, *12*(2), 147–153, doi:10.1007/s10291-007-0086-4.

Williams, S. D. P., Y. Bock, P. Fang, P. Jamason, R. M. Nikolaidis, L. Prawirodirdjo, M. Miller, and D. J. Johnson (2004), Error analysis of continuous GPS position time series, *J. Geophys. Res.*, *109*, B03412, doi:10.1029/2003JB002741.

Wyatt, F. K. (1982), Displacement of surface monuments: Horizontal motion, *J. Geophys. Res.*, *87*(B2), 979–989, doi:10.1029/JB087iB02p00979.

Wyatt, F. K. (1989), Displacement of surface monuments: Vertical motion, *J. Geophys. Res.*, *94*(B2), 1655–1664, doi:10.1029/JB094iB02p01655.

Zhang, J., Y. Bock, H. Johnson, P. Fang, S. Williams, J. Genrich, S. Wdowinski, and J. Behr (1997), Southern California Permanent GPS Geodetic Array: Error analysis of daily position estimates and site velocities, *J. Geophys. Res.*, *102*(B8), 18,035–18,055.

M. Hackl, Department of Earth and Environmental Sciences, Ludwig-Maximilians-Universität, Theresienstr. 41, D-80333 Munich, Germany. (hackl@geophysik.uni-muenchen.de)

U. Hugentobler, Institute for Astronomical and Physical Geodesy, Technische Universität München, D-80333 Munich, Germany.

R. Malservisi, Department of Geology, University of South Florida, 4202 E. Fowler Ave., SCA 528, Tampa, FL 33620, USA.

R. Wonnacott, Chief Directorate: National Geo-spatial Information, Mowbray, Cape Town 7705, South Africa.